International Journal of Steel Structures (2022) 22(4):1069–1085
https://doi.org/10.1007/s13296-022-00623-0

Online ISSN 2093-6311
Print ISSN 1598-2351

Mechanical Behavior of Laminated Rubber Isolation Bearing with Buckling Steel Plate

Jianpeng Sun[1] · **Gaolin Zhufu**[1]

Received: 15 December 2021 / Accepted: 2 June 2022 / Published online: 25 June 2022

Abstract
To improve the ability of disaster prevention and mitigation of bridges and realize the seismic resilience of traffic, this paper combines the elastic buckling characteristics of steel plates with the mechanical properties of laminated rubber bearings based on the principle of seismic isolation, and proposes a steel plate-laminated rubber composite seismic isolation bearing. The mechanical properties of steel plates were analyzed by ABAQUS software, and it was found that the shear stiffness of the steel plates before and after buckling had bilinear characteristics. The stiffness of the steel plate, the stiffness ratio before and after buckling, and the critical buckling load decreased with the increase of height-width ratio. According to the numerical regression, the precise formulas of the initial shear stiffness, the stiffness ratio before and after buckling, and the critical buckling load of the steel plate are proposed. Finally, by studying the seismic performance parameters of the alternative seismic isolation bearing, such as dissipation energy, shear stiffness, and equivalent viscous damping coefficient, the results show that the outer steel plate of the alternative type of bearing is in parallel with the rubber. The peripheral steel plate improves the overall energy dissipation capacity of the bearing. Under reciprocating load, the bearing exhibits three-stage characteristics, which can meet the performance requirements of bridge earthquake prevention and disaster reduction.

Keywords Seismic isolation · Steel plate · Buckling · Laminated rubber bearing · Shear stiffness · Height-width ratio

1 Introduction

As a control project of transportation infrastructure, the bridge is one of the lifeline projects of earthquake relief. For nearly a century, bridge seismic resistance has been an important research direction bridge engineering. Since the 1970s, significant progress has been made in theoretical research and engineering application of bridge seismic isolation technology (Yan et al., 2017). At present, the bearings used in the seismic design of bridge engineering are mainly laminated rubber bearings (Bhuiyan & Ahmed, 2007; Dario, 2003; Gent & Meinecke, 1970; Koh & Kelly, 1998; Tsai & Hsueh, 2001; Wang et al., 2014), sliding friction bearings (Fan et al., 2014; Pranesh & Sinha, 2000; Tsai et al., 2003, 2005; Tyler, 1977), lead rubber bearings (Robinson, 1982; Yan et al., 2020), hyperbolic spherical bearings (Tianbo et al., 2007), cable damping bearings (Wancheng et al., 2010). These seismic isolation bearings can not only effectively play the role of seismic isolation, but also improve the structural performance of bridge structure after the earthquake, and meet the rapid recovery of bridge function after the earthquake (Jian-zhong & Zhong-guo, 2017; Xilin et al., 2019). With the deepening of the understanding of earthquake disasters, the methods and theories of bridge seismic fortification have also been continuously improved. The focus of bridge seismic research has gradually shifted to seismic toughness with resilience, easy repair, and avoiding brittle failure (Wan-cheng et al., 2021). Seismic resilience emphasizes the functional recoverability of bridges, but if the seismic measures with stability are cumbersome and inefficient, it is challenging to be popularized. Therefore, it is of great engineering significance to design a bridge seismic resilience isolation device with a simple structure, apparent mechanical behavior, and excellent isolation effect.

As an efficient structural member, steel plate is widely used in high-rise and super high-rise structures due to its

✉ Gaolin Zhufu
1186879656@qq.com

Jianpeng Sun
sunjianpeng2001@163.com

[1] School of Civil Engineering, Xi'an University of Architecture and Technology, Xi'an 710055, Shaanxi, China

superior energy dissipation and good ductility. A lot of research reveals that the hysteresis curve of steel plate has an evident pinch appears. Tian Jie et al. (Jie et al., 2014; Shenggang et al., 2016; Zhouyi et al., 2019) found that a small amount of ultra-low yield point steel in the structure can achieve a significant seismic isolation effect. Liu Weiqing et al. (Weiqing et al., 2016; Wang et al., 2020; Weiqing et al., 2016; Sun et al., 2021, 2022a, b) designed different forms of structural energy dissipation devices by using this pinching characteristic. Saadatnia and Sheikhi combined rubber bearings with toughness damping devices for energy dissipation (Saadatnia et al., 2019; Wang & Bi, 2019). F. Sutcu et al. found that perforated buckling steel plate shear walls can improve the strength and ductility of the reinforced concrete frames to achieve sufficient seismic performance level (Sheikhi et al., 2020).

To conform to the concept of seismic resilience, this paper puts forward the design concept of seismic isolation bearing similar to a fuse. An alternative type of steel plate-laminated rubber composite seismic isolation bearing is proposed by replacing the lead rod in lead rubber bearing with peripheral shear steel plate. The mechanical properties of steel plates before and after buckling and the mechanical properties of the alternative bearing are studied emphatically. The peripheral steel plate can not only provide high horizontal shear stiffness, but also dissipate energy through hysteresis as a non-critical component in the earthquake to protect the key features, and it is easy to replace after the quake.

2 Steel Plate-Laminated Rubber Composite Isolation Bearing

The alternative type of bearing comprises of the peripheral steel plate and laminated rubber bearing, mainly including: upper (lower) cover plate, laminated rubber bearing, peripheral steel plate, etc. In addition, there is no contact between the peripheral steel plate and the laminated rubber, and the peripheral steel plate is welded with the upper cover plate and the lower cover plate. The alternative type of bearing structure is shown in Fig. 1.

The seismic isolation mechanism of the alternative bearing: In regular use, the laminated rubber in the bearing has sufficient vertical bearing capacity, and the peripheral steel plate provides sufficient horizontal shear stiffness, which can make up for the lack of shear stiffness of the bearing under the action of temperature, automobile braking force and concrete creep. Under a small earthquake, the peripheral steel plate is in the elastic stage, and the whole bearing is in the isolation state with self-resetting ability. Under the action of the medium earthquake, the outer steel plate is in the elastic buckling stage, and the local out-of-plane buckling occurs in the compression zone. However, it can still be restored under the act of reciprocating earthquake load, so it also has the ability of self-reset. Under the action of large earthquakes, the peripheral steel plate is in the elastic–plastic and plastic stages, and the seismic force transmitted by the substructure of the bridge is dissipated by reciprocating elastic–plastic deformation, and the whole bearing is in a damping state.

This alternative type of seismic isolation bearing can effectively compensate for the disadvantage of insufficient shear resistance of rubber bearing, and prevent the block from being damaged or even falling off the beam due to the out-of-control of horizontal displacement. Moreover, the bearing dissipates energy through the hysteresis

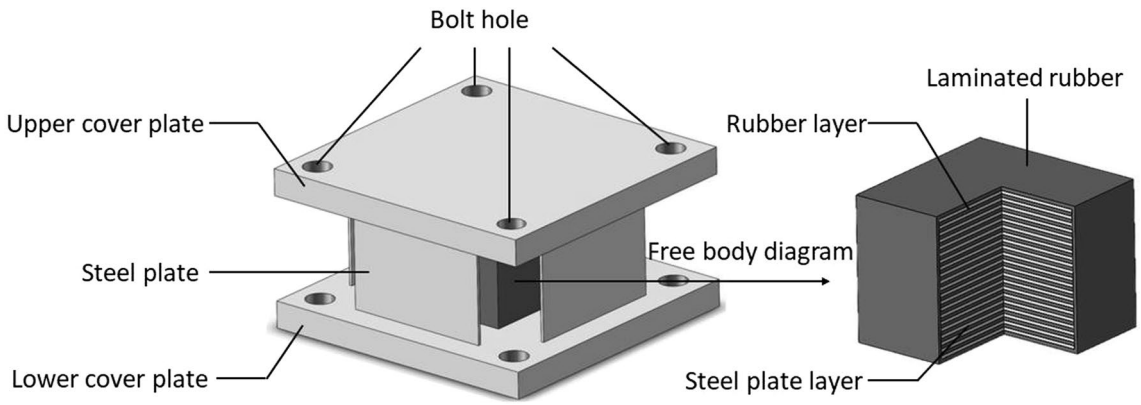

Fig. 1 Structural form of steel plate-laminated rubber composite isolation bearing

of steel plates under strong earthquakes without losing its damping capacity. In addition, the elastic and elastic buckling stage of steel plates has the self-centering ability, which conforms to the resilience of seismic toughness; the rapid replacement of scrapped steel plates after major earthquakes conforms to the easy reparability in seismic toughness.

3 Mechanical Properties of Steel Plate

3.1 First-Order Buckling Mode

Based on the seismic isolation mechanism of the alternative bearing, this paper uses ABAQUS finite element software to analyze the mechanical properties of the peripheral steel plate. The material of the steel plate is defined as Q235 steel. The elastic modulus is $E = 2.06 \times 10^{11}$ Pa, and the Poisson's ratio is 0.3. The constitutive model of steel plate is a bilinear kinematic hardening model and simulated by C3D8R element. To study the effect of the height-width ratio ($\beta = H/L$) on the mechanical properties of the steel plate, the thickness of the steel plate is controlled to be 5 mm, the width is 200 mm, and only the height of the steel plate is changed. When the boundary conditions are established, the lower end of the steel plate is completely fixed, the upper side only releases the degree of freedom in the X direction, and there is no constraint on both sides. Considering the geometric nonlinearity, the first-order buckling mode of the steel plate is applied as the initial defect of the steel plate. The unit load applied in the X direction on the upper side of steel plate. The first-order buckling modal diagram of steel plates with different height-width ratios under horizontal load is shown in Fig. 2.

It can be seen from Fig. 2 that the out-of-plane instability of steel plate will occur under horizontal load. Because there is no constraint on both sides of the steel plate, out-of-plane deformation occurs along the edge of both sides. With the increase of height-width ratio ($\beta = H/L$), the buckling wavelength of the free edge increases. At this time, the steel plate loses its stiffness, and the bearing capacity is temporarily lost. When the load reverses, the direction of the buckling half-wave changes accordingly, and the bearing capacity is gradually restored after the new buckling half-wave is formed (Sutcu et al., 2020).

3.2 Load–Displacement Curve

To study the influence of height–width ratio ($\beta = H/L$) on the mechanical properties of steel plates, six groups of steel plates with different sizes were monotonically loaded, and the load–displacement curves at the buckling wave crest and the whole steel plate were extracted respectively, as shown in Fig. 3.

It can be seen from Fig. 3 that when the load reaches a specific value, the steel plate will undergo out-of-plane buckling, and the shear stiffness will also decrease. With the increase of the height-width ratio, the critical buckling load of the steel plate decreases, and the steel plate is easy to enter the elastic buckling stage. However, the larger the height-width ratio is, the elastic stage of the steel plate will be significantly shortened, and the initial shear stiffness will be reduced to a large extent, which is unfavorable for the overall force of the structure. Therefore, the economic applicability should be taken as the criterion.

At the beginning of loading, the steel plate is in the elastic stage, only in-plane deformation. When loaded to the critical load, the steel plate enters the elastic buckling stage. With the increase of load, the steel plate enters the plastic stage again, resulting in sizeable out-of-plane deformation. Its energy dissipation capacity increases with the rise of plastic deformation until complete failure.

According to the results of finite element calculation, the initial shear stiffness (K_1), post-buckling shear stiffness (K_2), pre-buckling and post-buckling shear stiffness ratio ($\eta = K_2/K_1$), and critical buckling load (Q_Y) of steel plates under horizontal load change with different height-width ratios ($\beta = H/L$), as shown in Figs. 4 and 5.

It can be seen from Table 2 and figure that the initial shear stiffness (K_1), post-buckling shear stiffness (K_2), and critical buckling load (Q_Y) of steel plate decrease gradually with the increase of height-width ratio β, and the decreasing trend slows down gradually to 0. It shows that the larger the height-width ratio, the lower the influence of shear stiffness and buckling load. The shear stiffness ratio (η) before and after buckling decreases approximately linearly with the increase of height-width ratio (β), which shows that the larger the height-width ratio is, the more significant the difference of stiffness before and after buckling is, and the more pronounced the pinch phenomenon of steel plate is.

4 Accurate Calculation Formula

4.1 The Calculation Formula of Initial Shear Stiffness

Referring to Technical Specification for Steel Plate Shear Walls (Yan-lin & Ming, 2011), the horizontal shear stiffness of the formula for the initial horizontal shear stiffness K_0 of two-sided consolidated non-stiffened steel plate shear walls, such as Eq. 1. The accurate Eq. 2 of horizontal shear stiffness is proposed by fitting the finite element calculation data. The calculation results of the formula are shown in Table 1.

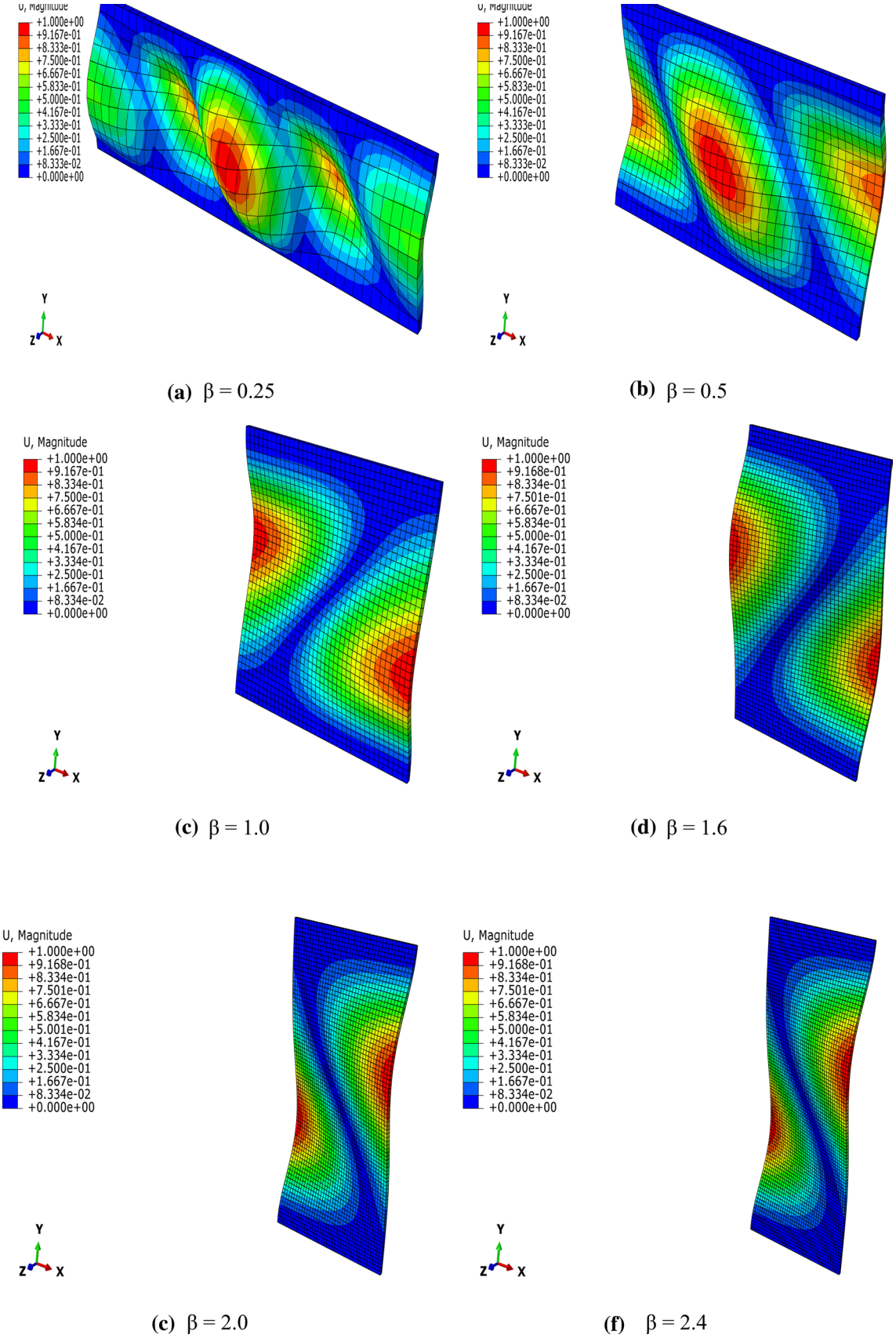

Fig. 2 First-order buckling mode

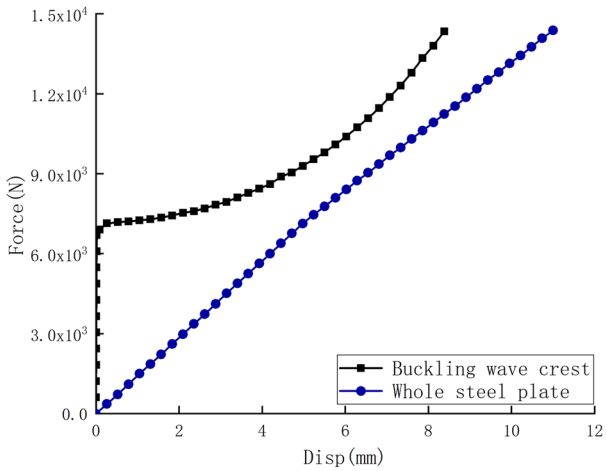

β = 0.25

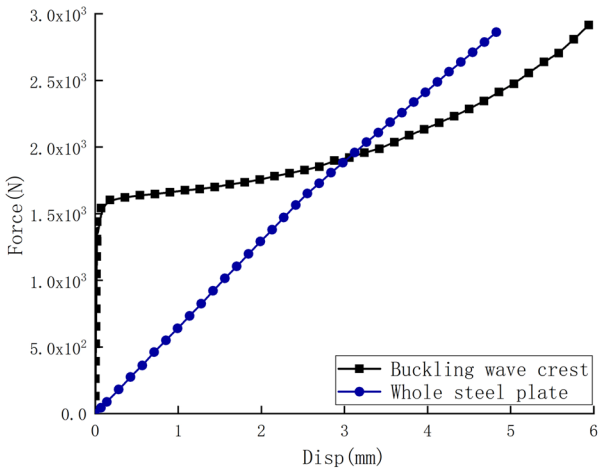

β = 0.5

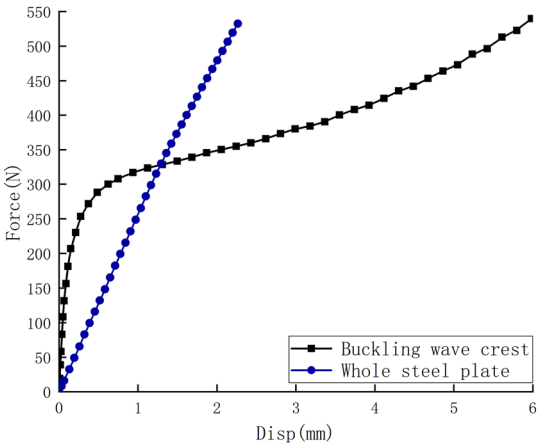

β = 1.0

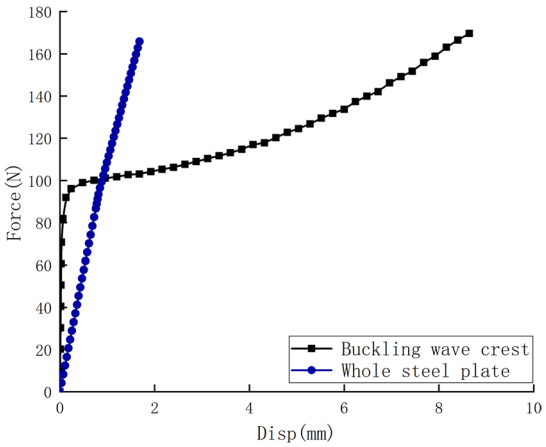

β = 1.6

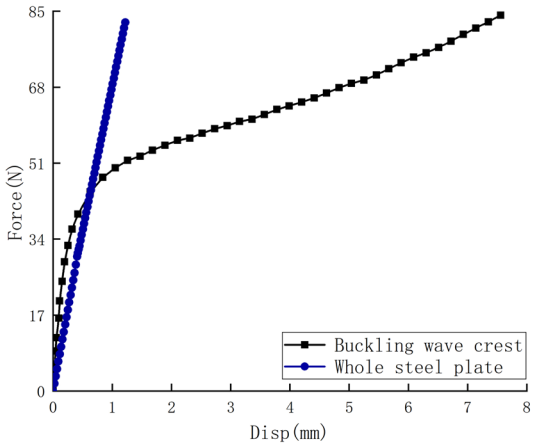

β = 2.0

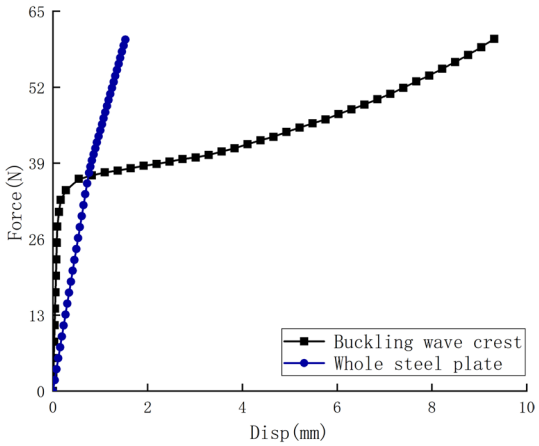

β = 2.4

Fig. 3 Load–displacement curve

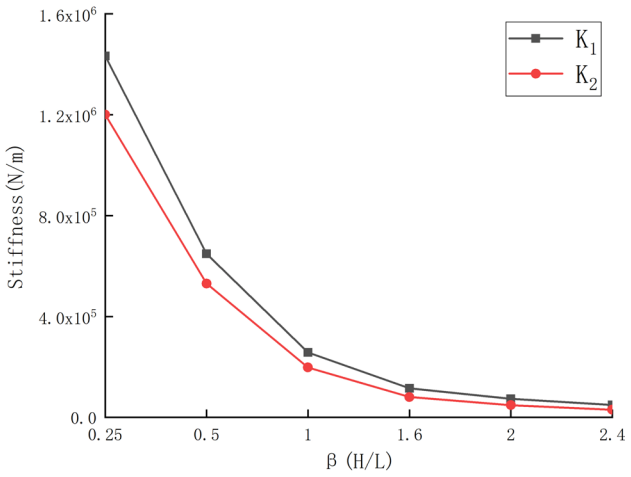

Fig. 4 Curves of β- K under horizontal loading

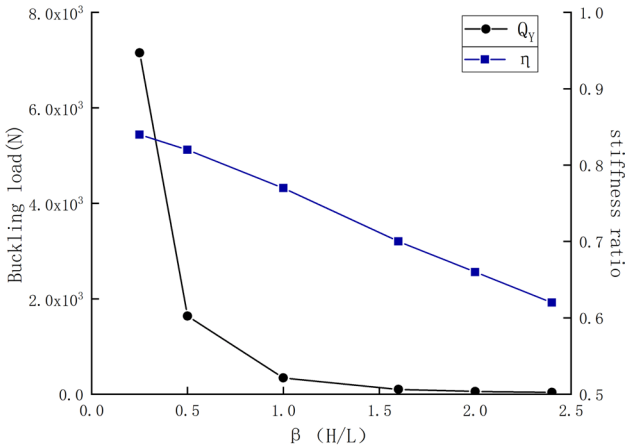

Fig. 5 Curves of β- Q_Y and β- η

$$K_0 = \frac{E \cdot t_w}{1/(L_e/H_e)^3 + 2.4 \cdot (1+\nu)/(L_e/H_e)} \tag{1}$$

$$K_0 = \frac{E \cdot t_w}{1/(L_e/H_e)^{2.94} + 2.3 \cdot (1+0.95\nu)/(L_e/H_e)^{1.05}} \tag{2}$$

where L_e is the net span of steel plate shear wall. H_e is the net height of steel plate shear wall; K_0 steel plate shear wall initial shear stiffness (N/mm). E is the elastic modulus of steel (N/mm^2). υ is the Poisson 's ratio of steel, generally taken 0.3. t_w is the thickness of the steel plate shear wall.

It can be seen from Table 2 that Eq. 1 can better calculate the initial horizontal shear stiffness of the steel plate connected to both sides. However, the error between the finite element value and the Eq. 1 value is relatively large, basically about 4–12%. Compared with the original formula, the error of the revised procedure is significantly reduced, and the error is reduced to less than 2%, which meets the accuracy of the research needs. This shows that the revised formula has high calculation accuracy.

4.2 The Calculation Formula of Stiffness Ratio Before and After Buckling

The existing research literature (JGJT, 2015) provides the shear stiffness ratio (η) calculation formula of steel plates before and after buckling, such as Eq. 3. An accurate stiffness ratio Eq. 4 is proposed by fitting the finite element calculation data. The calculation results of the formula are shown in Table 2.

$$\eta = 0.14\ln\left(L_e/H_e\right) - 0.118\ln\left(H_e/t_w\right) + 1.24 \tag{3}$$

$$\eta = 0.1\ln\left[6 + 0.158\left(H_e/t_w\right)\right] - 1.012\ln\left[3.5 + 0.75\left(H_e/L_e\right)\right] + 1.93 \tag{4}$$

It can be seen from Table 2 that the calculation error of the formula proposed in Reference (Yan-lin & Ming, 2011) is within 14%. The improved formula proposed in this paper can effectively reduce the error and control the error within 5%, thus verifying the accuracy of Eq. 4.

Table 1 Initial shear stiffness of steel side plate (K_1)

Groups	H/L	K_1(N/m)			Error (%)	
		Finite element solution	Form (1)	Form (2)	Form (1)	Form (2)
1	0.25	1,432,298.80	1,256,873.53	1,415,678.67	12.25	1.16
2	0.50	648,121.84	593,471.81	641,963.64	8.43	0.95
3	1.00	257,057.13	242,718.45	252,812.54	5.58	1.65
4	1.60	115,543.70	110,035.21	113,335.65	4.77	1.91
5	2.00	73,630.90	70,224.72	72,497.58	4.63	1.54
6	2.40	49,414.20	46,921.92	48,715.89	5.04	1.41

Error = (finite element value − formula value/(formula value)) × 100%

Table 2 Stiffness ratio of steel plate before and after buckling (η)

Groups	η			Error (%)	
	Finite element solution	Form (4)	Form (3)	Form (4)	Form (3)
1	0.84	0.88	0.84	4.71	0.10
2	0.82	0.79	0.82	3.89	0.29
3	0.81	0.7	0.77	13.76	4.18
4	0.7	0.63	0.71	9.35	1.17
5	0.66	0.61	0.66	8.32	0.60
6	0.62	0.58	0.62	6.29	0.08

Error = (finite element value − formula value/(formula value)) × 100%

Table 3 Stiffness ratio of steel plate before and after buckling (η)

Groups	H_e/t_w	H_e/L_e	Q_Y(N)		Error (%)
			Finite element solution	Form (5)	
1	25.00	0.25	7153.08	7235.92	1.16
2	50.00	0.50	1638.67	1585.76	-3.23
3	100.00	1.00	342.27	341.48	-0.23
4	160.00	1.60	101.54	104.47	2.88
5	200.00	2.00	58.62	59.53	1.56
6	240.00	2.40	37.88	37.60	-0.73

Error = (finite element value − formula value/(formula value)) × 100%

4.3 Calculation Formula of Critical Buckling Load

Through the numerical regression of the critical buckling load calculated by the finite element method, and according to the empirical formula of the existing research literature, the calculation formula of the buckling load of the two-side consolidated steel plate is obtained, as Eq. 5. To further verify the accuracy of the formula, Table 3 lists the results of finite element calculation and Eq. 5.

$$Q_Y = \begin{cases} \dfrac{\pi E L_e t_w}{4520}\left(\dfrac{H_e}{L_e}\right)^{-2.19}\dfrac{H_e}{L_e} \le 1 \\ \dfrac{\pi E L_e t_w}{4600}\left(\dfrac{H_e}{L_e}\right)^{-2.52}\dfrac{H_e}{L_e} > 1 \end{cases} \tag{5}$$

It can be seen from Table 3 that the data obtained from the calculation Eq. 5 of the critical the buckling load of the steel plate with opposite consolidation and opposite freedom proposed in this paper and the results of the finite element numerical analysis is controlled within 2.88%. It can be said that the proposed calculation Eq. 5 is relatively accurate.

5 Mechanical Properties of Alternative Type Seismic Isolation Bearing

5.1 Equivalent Model of Alternative Type Seismic Isolation Bearing

For the alternative type seismic isolation bearing proposed in this paper, the equivalent simplified model of the structure is shown in Fig. 6. Vertical stiffness K_w is mainly provided by laminated rubber. The laminated rubber and the external steel plate are parallel systems, so the horizontal shear stiffness is provided by the steel plate and the laminated rubber together. It is assumed that the total stiffness of the horizontal lateral resistance is the sum of the steel plate stiffness K_0 and the laminated rubber bearing K_h, and the damping is C. To verify this view, the modeling stress analysis of the alternative bearing is carried out.

5.2 Finite Element Modeling of the Alternative Type Bearing

The steel plate is divided into the thin plate ($\lambda > 300$), medium-thick plate ($300 \ge \lambda \ge 100$), and thick plate ($\lambda \le 100$) according to its height-thickness ratio (λ). The thick plate is dominated by energy consumption, but the self-centering ability is not reasonable under reciprocating load. The elastic buckling of the thin steel plate is very prominent, but the energy consumption level will decrease, and the medium-thick plate has both characteristics. To provide sufficient lateral stiffness and control the height-thickness ratio of the steel plate, the steel plate can be stratified along the thickness direction during modeling. After delamination, the horizontal shear stiffness is equal to the sum of the stiffness of each layer, and the elastic buckling becomes evident with the increase of the height-thickness ratio of each layer. In this paper, the double-layer steel plate is established to control the height-thickness ratio and shear stiffness. The ABAQUS finite element model of the bearing is shown in Fig. 7.

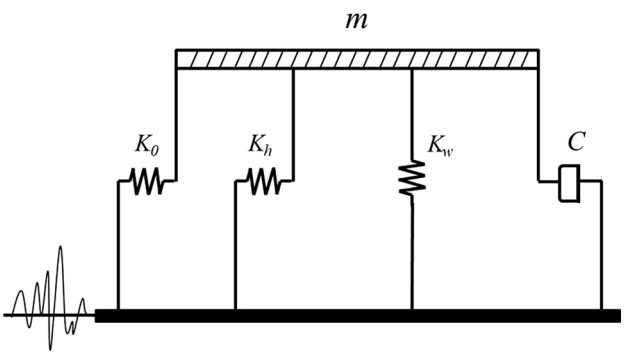

Fig. 6 Equivalent model of alternative type bearing

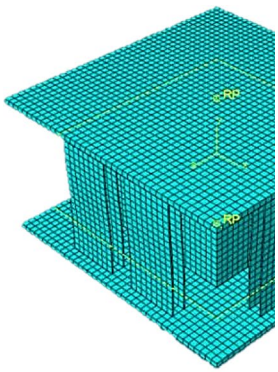

Fig. 7 Finite element model

(a) Alternative typ

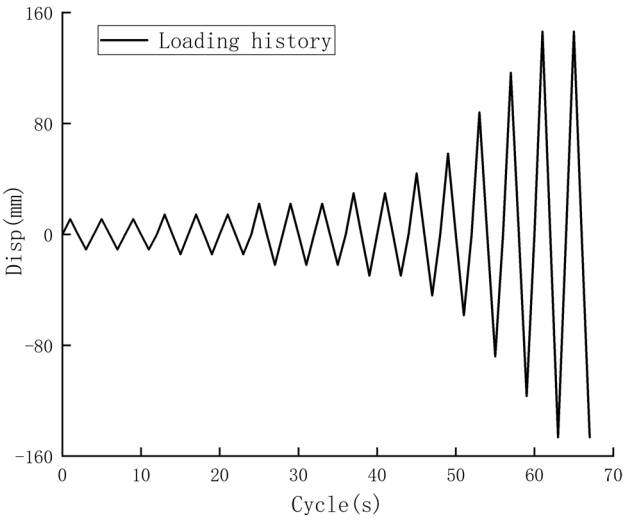

Fig. 8 Loading history

According to the size of steel plate shear wall in Reference (Sutcu et al., 2020), considering the influence of the thickness of rubber and embedded steel plate, the alternative bearing size was determined: the thickness of the external steel plate was 5 mm, the height was 500 mm, the width was 200 mm, and the height-width ratio was $\beta = 2.5$. The height of the steel plate corresponds to the height of the support. Laminated rubber bearing parameters: rubber plane size 500 mm × 500 mm, shear modulus 0.8 N/mm^2; embedded steel plate plane size 490 mm × 490 mm, thickness 5 mm, a total of 20 layers; the thickness of rubber layer between embedded steel plates is 20 mm, a total of 19 layers; the plane size of the upper and lower cover plates is 1000 mm × 1000 mm, the thickness is 20 mm, and the thickness of the rubber layer in contact with the upper and lower cover plates is 10 mm. The first shape coefficient of rubber bearing is 6.13. For the mechanical properties of minor strain and medium strain, Mooney-Rivilin constitutive model (Tsai et al., 2003) was used to simulate the rubber material with C3D8RH substantial component. The steel plate was made of Q235 steel with elastic modulus $E = 2.06 \times 10^{11}$ Pa and Poisson's ratio of 0.3. The C3D8R solid element was used to simulate. Considering the influence of the vertical load and displacement on the horizontal shear effect of the peripheral steel plate in the actual situation, the first-order buckling mode of the steel plate was used as the initial defect (pre-deformation). The connection between rubber, steel plate, and upper and lower cover plates is simulated by 'Tie'.

5.3 Analysis Result

The seismic action is simulated by reciprocating displacement loading through the support, and the displacement loading process is shown in Fig. 8. The alternative bearing hysteresis curve and skeleton curve are shown in Fig. 9**.**

It can be seen from Fig. 9 that the hysteresis curve of the alternative type bearing has a long sliding section, which reflects that the internal laminated rubber has good horizontal displacement ability and can increase the natural vibration period of the structure. There is a particular pinch phenomenon in the middle, but its envelope curve area is large, which does not affect its seismic energy dissipation capacity. Moreover, the alternative bearing has the self-centering ability through the elastic buckling characteristics of the peripheral steel plate, and realizes the functional recovery of the structure, which conforms to the concept of seismic toughness (Liang et al., 2018). The skeleton curve of alternative bearing presents three-stage characteristics:

1. Initial elastic stage: The overall shear stiffness of the alternative type bearing is approximately the sum of the shear stiffness of the peripheral steel plate and the laminated rubber bearing.
2. Elastic buckling stage: This stage reflects the geometric nonlinearity of the outer steel plate; the steel plate has local buckling instability and loses stiffness.
3. Plastic stage: Due to the large displacement load, the steel plate in the Y direction shows certain flexibility, and the steel plate in the X direction consumes energy through reciprocating plastic deformation.

The boundary between the above three stages is evident, indicating that the alternative bearing meets the stiffness requirements of the regular use and ultimate bearing capacity of the seismic isolation device.

The representative lead-rubber bearings are widely used in bridge seismic resistance because of their excellent seismic isolation ability. The lead core is the primary energy dissipation component, which provides the necessary damping for the bearings. But under the action of severe ground motion, the lead body will deform, thus losing work

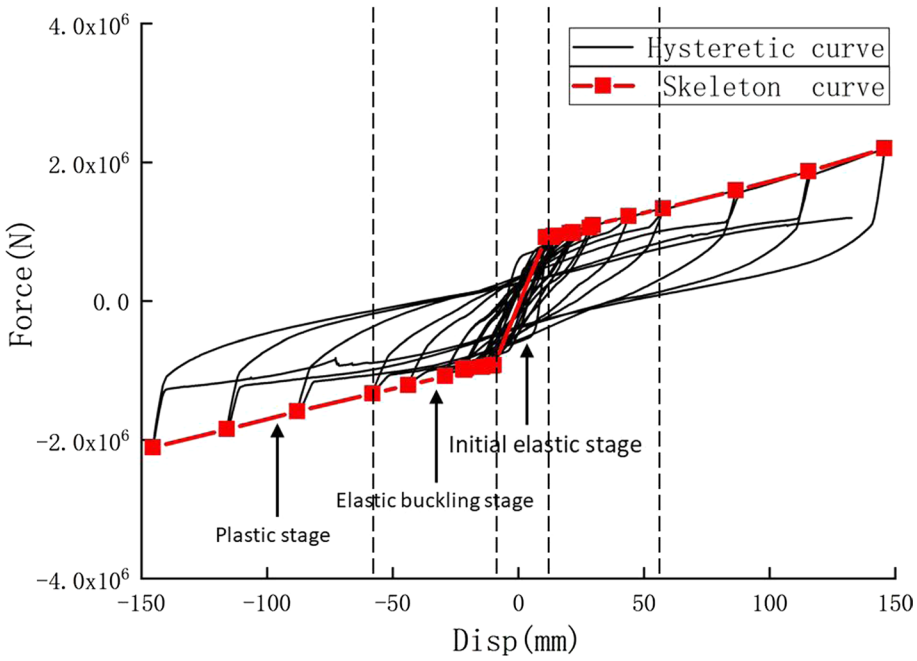

Fig. 9 Hysteresis curve of alternative type bearing

efficiency. However, the lead body is located in the rubber and steel layers and is difficult to replace after the earthquake. Comparing the hysteresis curve of the alternative bearing with that of the lead rubber bearing in Reference (Wang & Bi, 2019), it is found that the hysteresis characteristics of the two are similar, showing a flat ring, which verifies the rationality of the design of the alternative bearing. The shear steel plate in this paper can achieve similar hysteretic characteristics with the lead rubber bearing. The shear steel plate can replace the lead core to improve damping and dissipate seismic energy, and the seismic isolation bearing with good performance is obtained by optimizing the parameters of the steel plate.

Hysteretic analysis of single steel plate and plate rubber under the same loading scheme is shown in Fig. 10. It can be seen that the steel plate enters the buckling under a low load. From the perspective of energy consumption, this phenomenon of rapidly entering the buckling stage is beneficial to the energy consumption of the structure. In addition, the overall pinching phenomenon of the hysteresis curve is pronounced. At the beginning of loading, the whole steel plate is elastic, and there is only in-plane deformation; when the steel plate is loaded to the critical load, the stiffness is reduced, which is due to the large aspect ratio of the selected steel plates and the absence of constraints on both sides. The out-of-plane deformation of the steel plate along the edge of the waist on both sides is faster, and the out-of-plane buckling instability of the steel plate occurs. With the rise of load, the steel plate enters into plasticity and produces large out-of-plane deformation. The energy consumption of steel plate increases with the increase of plastic deformation until it is destroyed. According to the specification 《test method for laminated rubber bearings GB-T20688》. The ultimate horizontal displacement of the standard laminated rubber bearing is 62.16 mm. From the hysteresis curve and skeleton curve of a single steel plate, it can be seen that the horizontal shear force required for the steel plate after the 14th hysteresis cycle (88 mm) decreases. The stress variation diagrams of the steel plate are extracted respectively. In Fig. 11 A–I are the stress contours, and their sizes increase in turn. In the elastic stage, the stress variation of the steel plate conforms to the tension and compression rod model, and the shape is diagonally symmetrical. With the increase of load, the shape is gradually expanded and staggered, and the steel plate only deforms in a plane. In the buckling stage, the stress contour forms a stress gradient along the buckling peaks on both sides, and the stress gradually increases. In the elastic stage, the other two diagonal shapes gradually extend from the curve to the value line. The whole plate forms a slight stress gradient along the buckling peak diagonal, and includes a large stress tension band along the remaining diagonal. In the plastic energy dissipation stage, with the increase of load, the whole plane undergoes out-of-plane deformation, showing a typical tension band. For example, in the figure, the E and F lines gradually change from diagonal distribution to oblique penetration through the whole steel plate. The C and D lines gradually change to the triangle area on both sides of the tension band. When the ultimate displacement of the standard rubber bearing is 62.16 mm, the outer steel plate of the composite system is in the elastic buckling stage, indicating that the steel plate

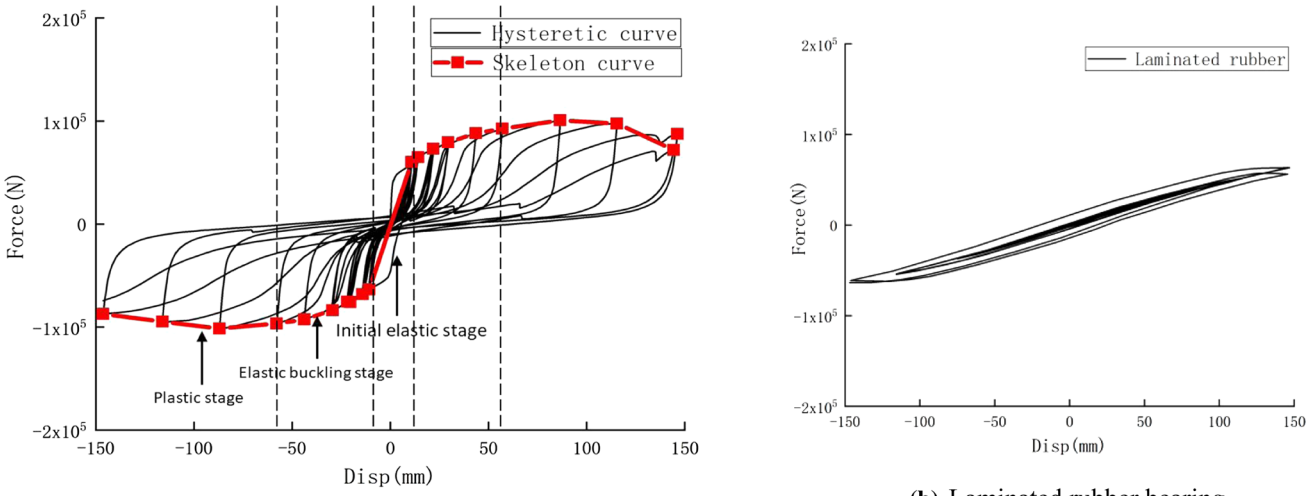

(a) Single steel plate

(b) Laminated rubber bearing

Fig. 10 Hysteresis curves of single steel plate and laminated rubber bearing

can adapt to the composite system under large deformation without plate failure.

Amount of dissipated energy (Ep) which is calculated by the sum of the area below a hysteretic curve is the first criterion for evaluating seismic performances of metallic dampers. Another critical parameter is the equivalent viscous damping coefficient (ζ_{eq}), representing the dissipated energy of equivalent viscous damping. The dissipation coefficient (E) is the ratio of the peak area surrounded by the hysteresis loop, the transverse coordinates corresponding to the peak, and the triangle surrounded by the three points of the origin, as shown in Fig. 12. According to the calculation formula, the variation law of the dissipation energy and equivalent viscous damping coefficient of the alternative bearing with the displacement cycle is calculated, as shown in Figs. 13 and 14.

$$E = \frac{S_{DEF} + S_{BFE}}{S_{DOC} + S_{AOB}} \tag{6}$$

$$\zeta_{eq} = \frac{1}{2\pi} \cdot \frac{S_{DEF} + S_{BFE}}{S_{DOC} + S_{AOB}} \tag{7}$$

where the $S_{DEF} + S_{BFE}$ is the area surrounded by hysteresis loop; $S_{DOC} + S_{AOB}$ is the sum of two triangle areas in the figure.

Figure 13 shows the variation of hysteretic energy dissipation and displacement value. The external steel plate has specific shear stiffness under initial loading, and the force required to push the steel plate horizontally is significant, so the area of the hysteresis loop is large in the first cycle. After buckling, the energy needed to push the external steel plate becomes smaller, and the area of the hysteresis loop decreases. With the increase of horizontal displacement, the outer steel plate enters the plastic energy dissipation stage, the area surrounded by the curve gradually increases, and the energy dissipation capacity gradually increases. It can be seen that the dissipation capacity of the alternative type bearing increases rapidly after reaching the plastic stage, from 50 to 300 kNm; in the initial elastic and elastic buckling stage, the dissipation capacity is maintained below 50 kNm. After the outer steel plate reaches the plastic state, combined with the energy dissipation capacities of laminated rubber bearing, the superposition of the two energy dissipation capacity dramatically improves the energy dissipation capacity of the steel plate-laminated rubber bearing.

Figure 14 shows the equivalent viscous damping coefficient and displacement variation. Based on the cumulative hysteretic response under the selected load history, the equal viscous damping coefficient of the composite bearing increases slowly, and remains between 10 and 20%. At this time, the outer steel plate is in the elastic buckling stage. When the horizontal displacement reaches the limit displacement value of laminated rubber bearing, the outer steel plate is in the plastic energy dissipation stage, and the equivalent viscous damping coefficient of the bearing reaches 19%. Over the limit displacement, some steel plates are damaged, and the viscous damping coefficient decreases slowly. Overall, the external steel plate consumes a large amount of lagging energy, so it has sufficient (ζ_{eq}) value for seismic application purposes.

In order to highlight the fullness of the hysteresis curve to reflect the energy dissipation capacity and pinching level of the structure, and improved parallelogram rule is proposed

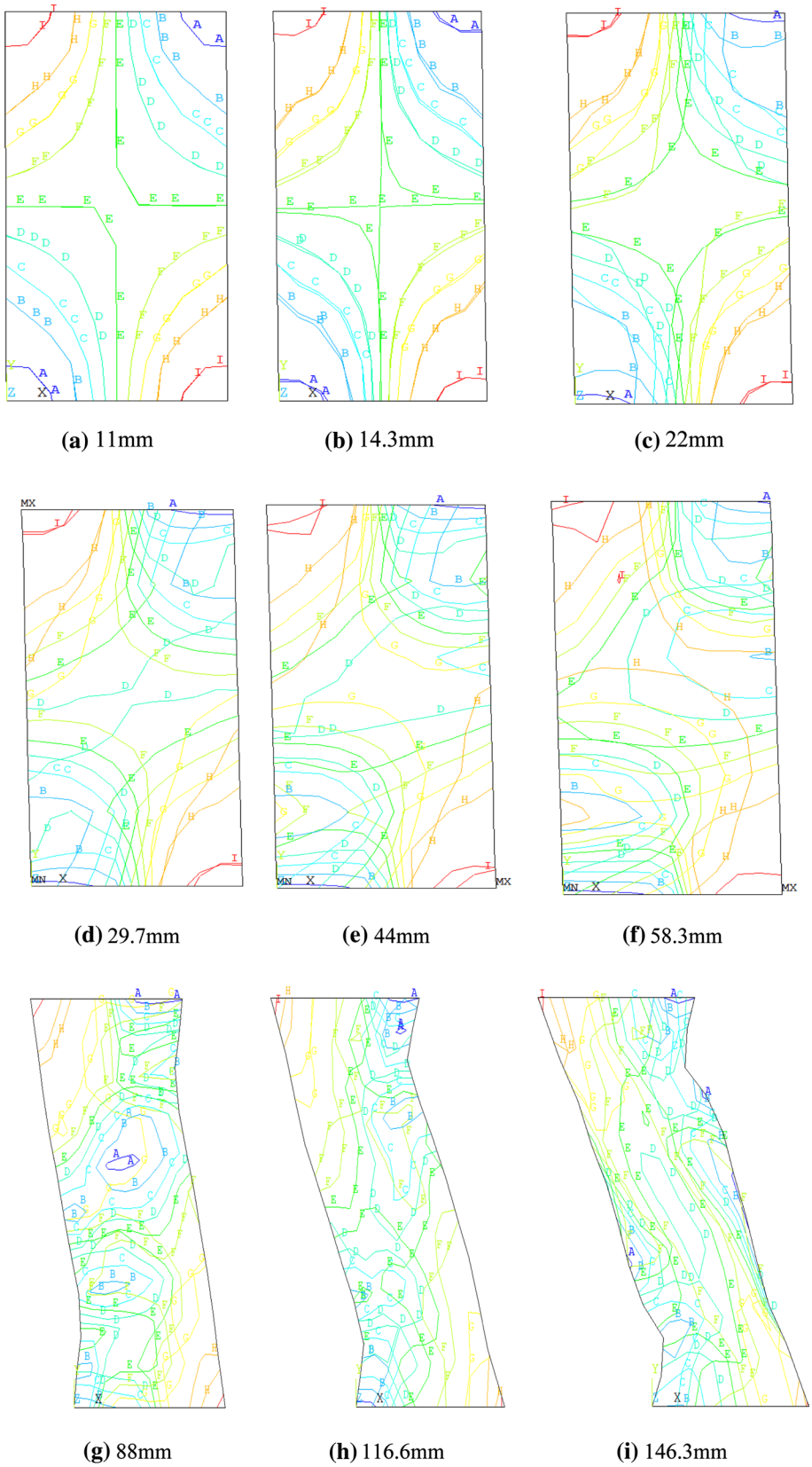

(a) 11mm **(b)** 14.3mm **(c)** 22mm

(d) 29.7mm **(e)** 44mm **(f)** 58.3mm

(g) 88mm **(h)** 116.6mm **(i)** 146.3mm

Fig. 11 Stress variation of single steel plate

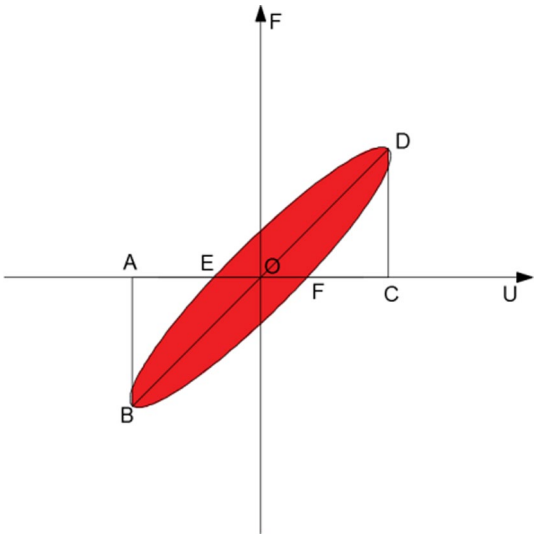

Fig. 12 Energy dissipation coefficient

in this paper. The method for determining the energy dissipation coefficient E is shown in Fig. 15. The red area is an area surrounded by a hysteresis loop, and the S_{ABCD} area is a parallelogram. The envelope area of the hysteresis curve of each component of the alternative bearing is calculated by the formula. The S_{ABCD} is 276.55 kNm, and the S_{AEBCGD} is 185.29 kNm. The overall energy consumption of the bearing is 185.29 kJ, and the energy consumption quantification coefficient E is 0.67. Similarly, the S_{ABCD} of a single steel plate is 35.14 kNm, S_{AEBCGD} is 22.49 kNm, the energy consumption of 8 steel plates in the horizontal direction is 179.89 kJ, accounting for 97.09% of the total energy consumption of the bearing, and the energy consumption quantization coefficient E is 0.64. Laminated rubber energy consumption is 5.4 kJ, accounting for 2.91%. It can be seen that under the same load conditions, the outer steel plate of the alternative bearing is the primary energy dissipation component, and the rubber energy dissipation capacity is small. It can be seen from the above that the peripheral steel plate of the alternative bearing improves the broad energy dissipation capacity of the bearing. The broad hysteresis curve of the alternative bearing is the sum of rubber and peripheral steel plate, which can be considered a parallel relationship between steel plate and rubber. The displacement load with monotonous shear direction is applied to the replaceable bearing. The finite element calculation shows that the total stiffness of the horizontal peripheral steel plate is 102 296.8 N/mm, the initial shear stiffness of the rubber is 0.5079 kN/mm, and the total stiffness of the alternative bearing is 108.7364 kN/mm. The horizontal shear load–displacement curve of the alternative bearing is shown in Fig. 16. From the above analysis: rubber shear stiffness is far less than the shear stiffness of the peripheral steel plate, less than 1% of the peripheral steel plate shear stiffness; the error between the sum of the rubber shear stiffness and the shear stiffness of the peripheral steel plate and the total stiffness of the support (total stiffness of the steel plate + rubber stiffness − total stiffness of the support/total stiffness of the support) is within 6%, indicating that the overall shear stiffness of the new support can be approximated by the sum of the shear stiffness of the peripheral steel plate and the laminated rubber support. It can be considered that there is a parallel relationship between steel plate and rubber.

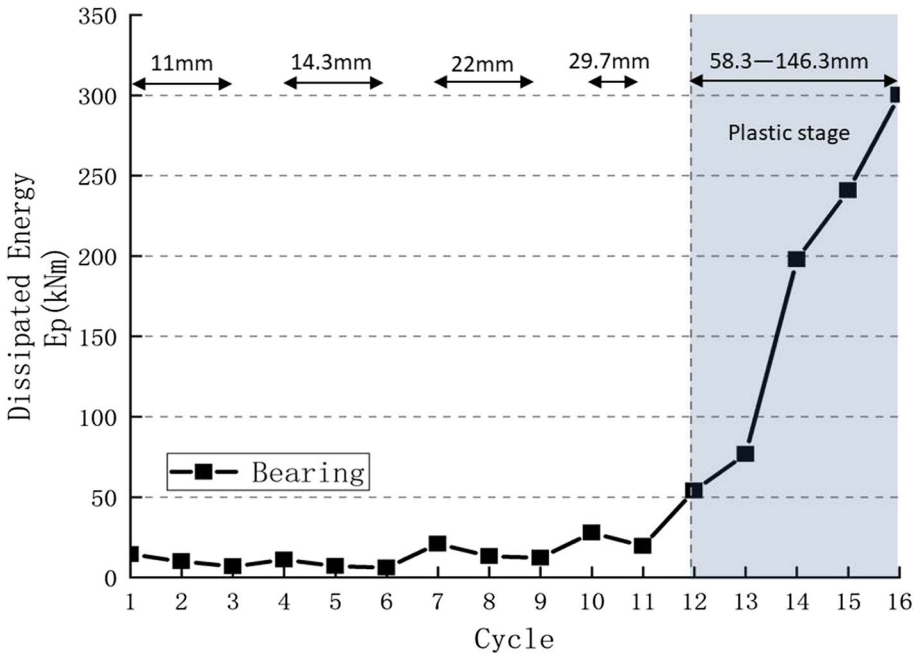

Fig. 13 Energy dissipation at each cycle for the alternative type bearing

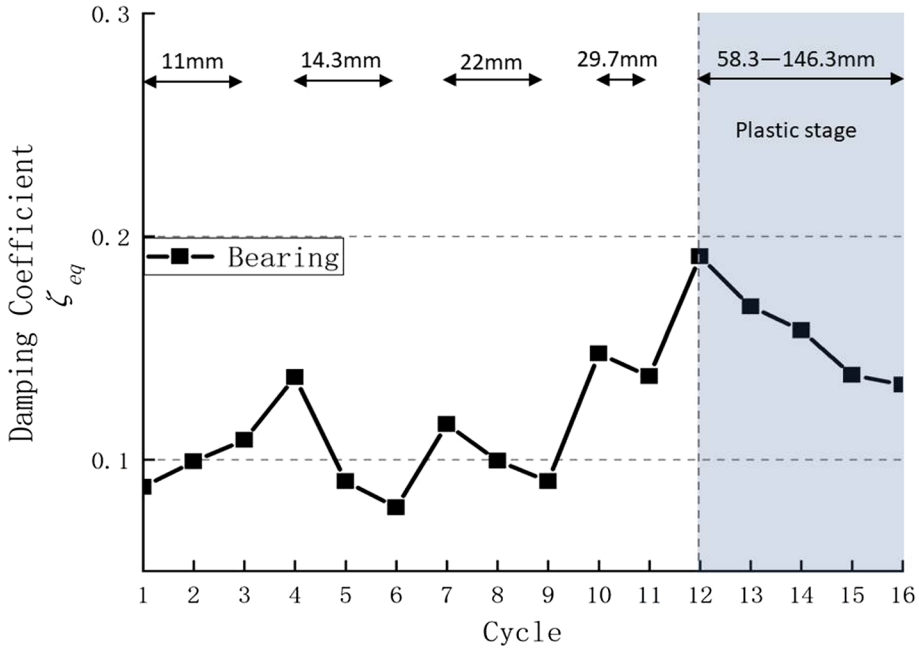

Fig. 14 Equivalent viscous damping coefficient for the alternative type bearing

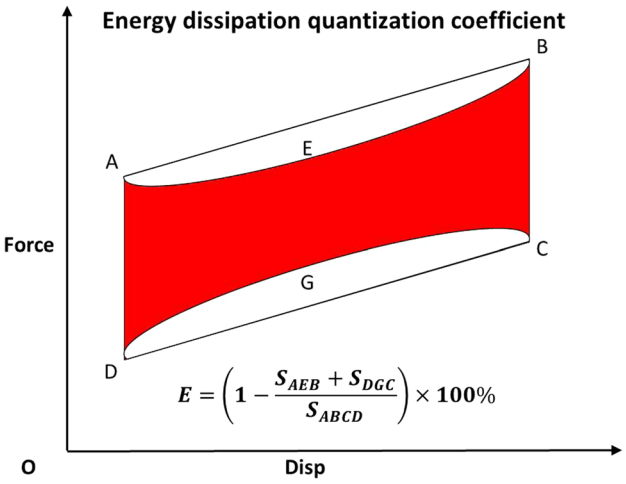

Fig. 15 Improved method of energy dissipation coefficient

5.4 Effect of Bidirectional Loading

The design of seismically isolated structures is an iterative procedure that starts with preliminary design to verification of the design. In the last step of design procedures, it is expected to perform detailed 3 dimensional (3D) analyses which take into account 2 or 3 dimensional strong ground motion effects. Thus, to show the behavioral differences, this part of the study involves the bearing behavior under bidirectional loading (Berman et al., 2004). The numerical analysis of the alternative type bearing was carried out under 0° and 45° loading directions, as shown in Fig. 17. When the support bears 0° load, the steel plates on both sides bear 0° shear load, and the other two bears 90° load. When the support bears a 45° load, all outer steel plates bear a 45° load. Therefore, the hysteresis performance of a single steel plate at 0° and 45 loading directions should be obtained first (Figs. 18, 19). Since the hysteresis curve under 0° load is plumper than that under 45° load, increasing the angle of loading direction will reduce the energy consumption. As shown in Fig. 20, although there are some deviations in the displacement cycle in the plastic stage, the hysteretic performance of the bearing under 0° and 45° loading is very similar, which is desirable in seismic design and retrofit application. It can be seen from Figs. 20 and 21 that the cumulative plastic energy dissipation difference of a single steel plate in 0° and 45° loading directions reach 21.7%. In contrast, the incremental plastic energy dissipation difference of the support composed of eight steel plates is 4.3%. Therefore, it can be obtained that the symmetric element damper can eliminate the different behaviors of a single steel plate under different loading directions.

6 Conclusions

Based on the design concept of bridge seismic isolation, this paper puts forward an alternative type of steel plate-laminated rubber composite seismic isolation bearing, studies the mechanical properties of the steel plate and alternative bearing, and draws the following conclusions:

1. The shear stiffness of the steel plate has prominent bilinear characteristics before and after buckling. The larger

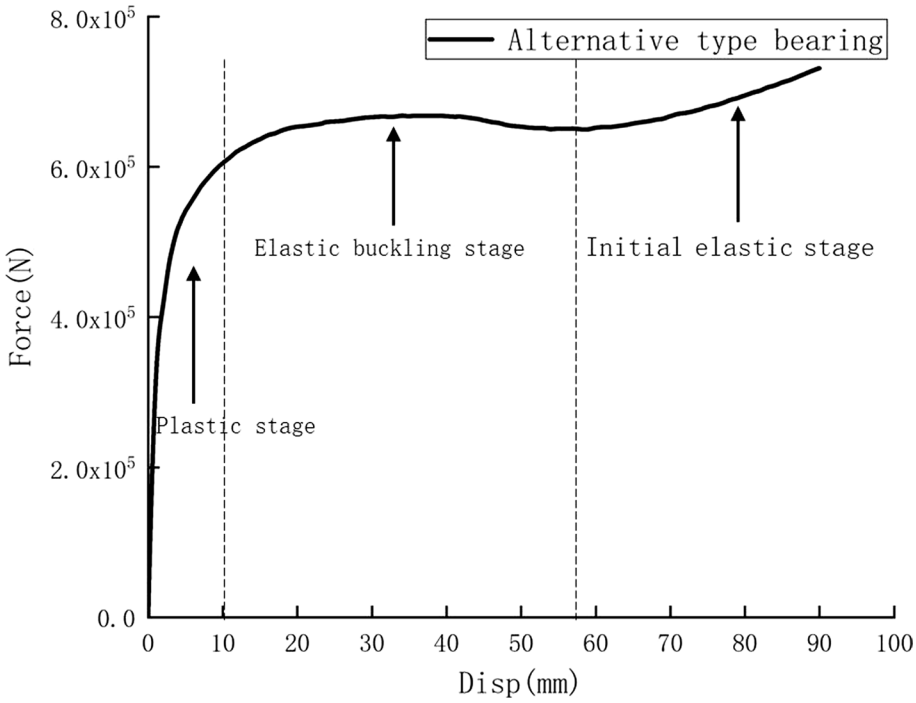

Fig. 16 Load–displacement curve of alternative type bearing under unidirectional loading

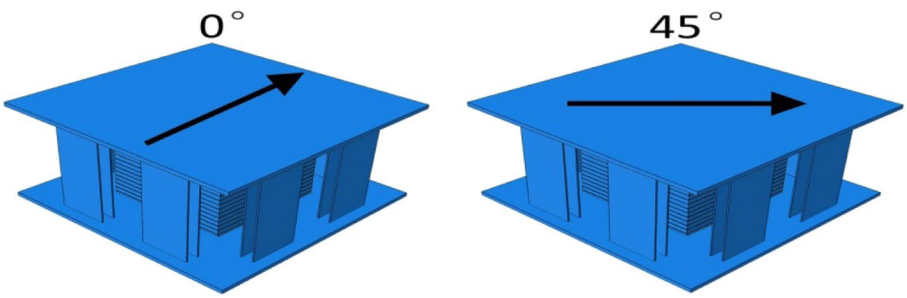

Fig. 17 Different loading directions

the aspect ratio is, the smaller the initial shear stiffness, post-buckling stiffness, and critical buckling load of the steel plate are, and the decreasing trend slows down sharply and gradually tends to 0. The shear stiffness ratio before and after buckling shows an approximately linear decreasing trend with the increase of aspect ratio, indicating that the larger the aspect ratio is, the more significant the stiffness difference before and after buckling is, and the more pronounced the pinching phenomenon of steel plate is.

2. Through the regression analysis of the mechanical parameters of the steel plate, the simplified calculation formulas of the initial horizontal shear stiffness, the shear stiffness ratio before and after buckling, and the first-order buckling load are proposed, and compared with the simulation analysis results, the accuracy of the formula is further verified.
3. In the alternative bearing, there is a parallel relationship between the outer steel plate and the rubber. The outer steel plate is the primary energy dissipation component, which can improve the energy dissipation capacity of the bearing. The shear stiffness of the bearing can be approximated to the sum of the shear stiffness of the outer steel plate and the laminated rubber. The skeleton curve of the alternative bearing shows three-stage characteristics of elasticity, elastic buckling, and plasticity, which can meet the requirements of more refined performance objectives.
4. By comparison, it is found that the hysteresis curve of the alternative bearing is similar to that of the lead rubber bearing. The shear steel plate of the alternative bearing can replace the lead core to improve damping and dissipate seismic energy. It is convenient to manufacture, place, and repair after failure, so it is more economical.
5. The dissipation energy of the alternative bearing increases with the increase of displacement, and

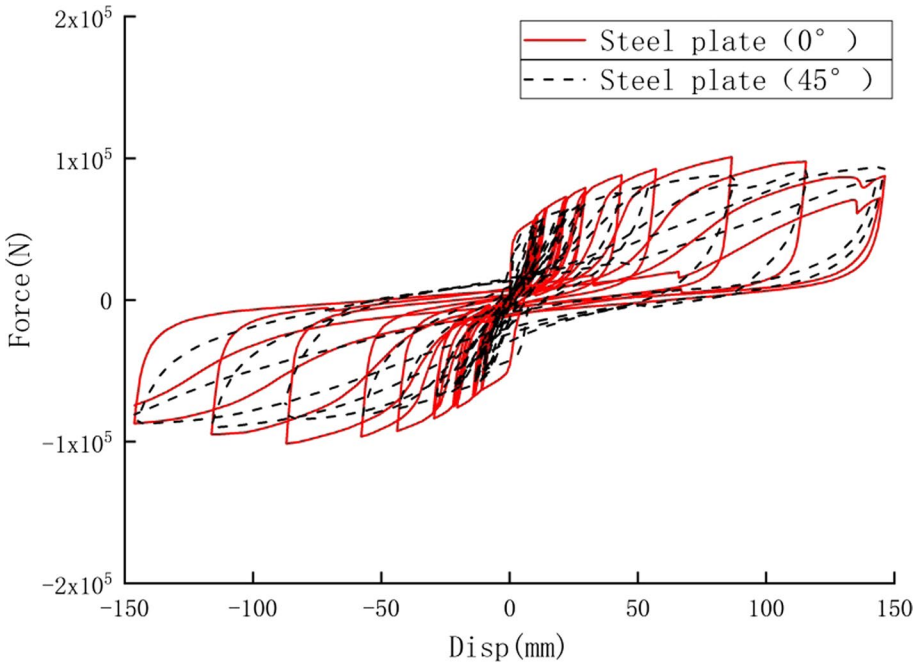

Fig. 18 Hysteretic curve of single steel plate under bidirectional loading

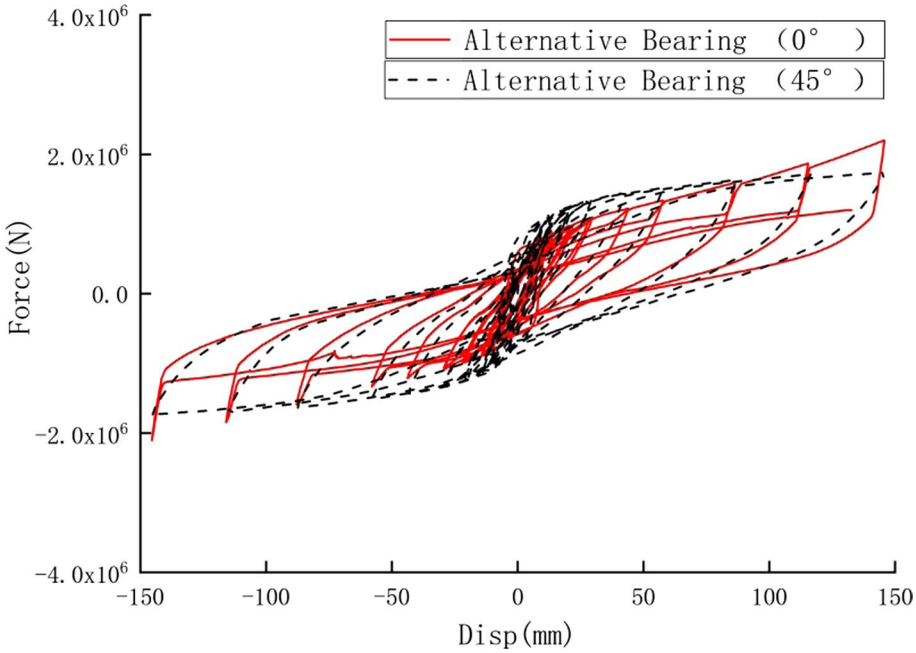

Fig. 19 Hysteretic curve of alternative type bearing plate under bidirectional loading

increases rapidly at large deformation. The equivalent viscous damping coefficient reaches 20% from 50 to 300 kNm, proving that the alternative bearing steel plate consumes a lot of energy.

6. The hysteretic behavior of steel plates and alternative bearing under bidirectional loading is also studied. The numerical analysis of different loading angles shows that when the symmetrical structure is used as a damper element, the dissipation energy, and equivalent viscous damping performance parameters change little.

It is believed that with the deepening of research and the rich theoretical system of seismic isolation, the mechanical properties of steel plate-laminated rubber composite seismic isolation bearing will have significant room for improvement in the future.

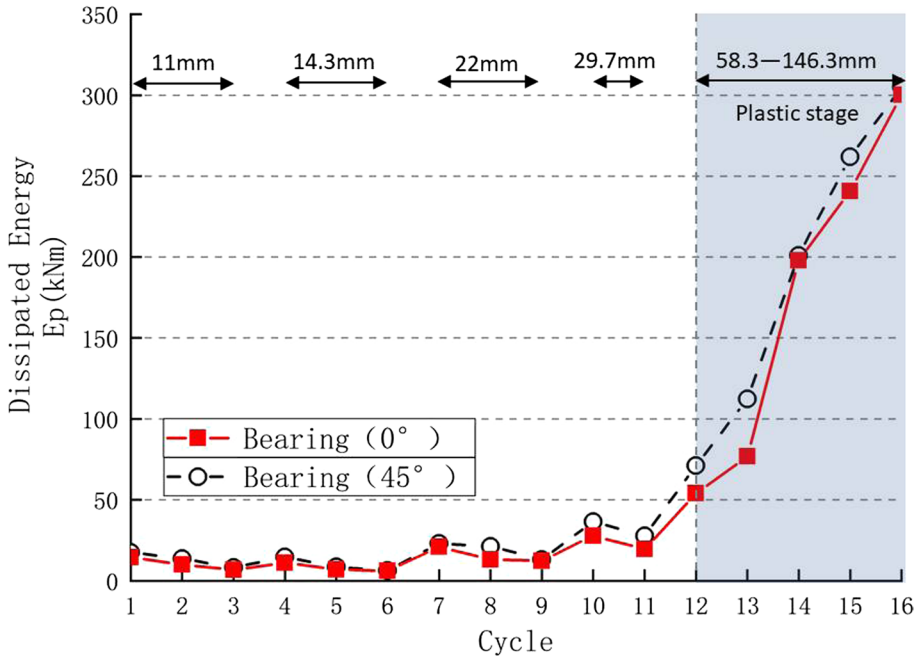

Fig. 20 Energy dissipation at each cycle for the alternative type bearing

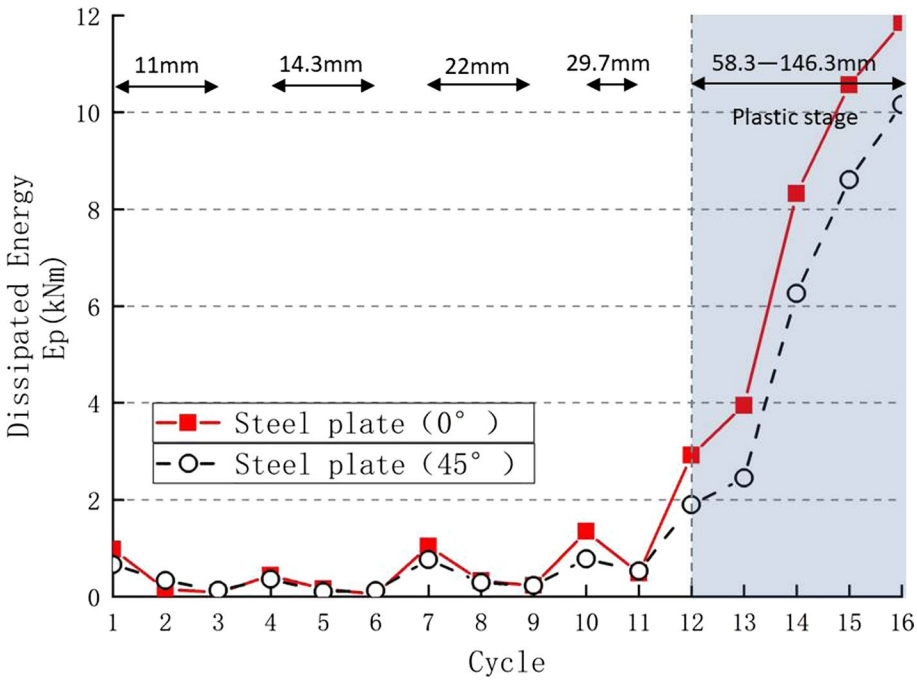

Fig. 21 Energy dissipation at each cycle for the single steel plate

Acknowledgements The study was jointly supported by the the Xian Science and Technology Innovation Talent Service Enterprise Project (Grant No. 2020KJRC0047), the Natural Science Foundation of Shaanxi Province (Grant No. 2020JM-475) and the National Natural Science Foundation of China (Grant No. 51408453). The authors gratefully acknowledge the financial support.

References

Berman, J. W., Celik, O. C., & Bruneau, M. (2004). Comparing hysteretic behavior of light-gauge steel plate shear walls and braced frames. *Engineering Structures, 27*(3), 475–485.

Bhuiyan, A. R., & Ahmed, E. (2007). Analytical expression for evaluating stress-deformation response of rubber layers under combined action of compression and shear. *Construction and Building Materials, 21*(9), 1860–1868.

Dario, A. O. J. (2003). Tension buckling, in multilayer elastomeric bearings by James M Kelly. *Journal of Engineering Mechanics, 129*(12), 1363–1368.

Fan, F., et al. (2014). Anti-seismic effect of lattice grid structure with friction pendulum bearings under the earthquake impact of various dimensions. *International Journal of Steel Structures, 14*(4), 777–784.

Gent, N., & Meinecke, E. A. (1970). Compression, bending, and shear of bonded rubber blocks. *Polymer Engineering and Science, 10*(1), 48–53.

JGJT 380–2015 (2015). Technical specification for steel plate shear wall. Ministry of housing and urban rural development of the people's Republic of China

Jian-zhong, L., & Zhong-guo, G. (2017). Research progress on bridge seismic design: Target from seismic alleviation to post-earthquake structural resilience. *China Journal of Highway and Transport, 30*(12), 1–9.

Koh, G., & Kelly, J. M. (1998). A simple mechanical model for elastomeric bearings used in base isolation. *International Journal of Mechanic Science, 30*(12), 933–943.

Meng, W., & Peng, B. (2019). *Study on seismic behavior and design method of dissipative bolted joint for steel frame with replaceable low yield point steel connected components* (p. 198). Elsevier Ltd.

Meng, W., Xiaokang, Z., Lu, Y., & Weiguo, Y. (2020). *Cyclic performance for low-yield point steel plate shear walls with diagonal T-shaped-stiffener* (p. 171). Elsevier Ltd.

Pranesh, M., & Sinha, R. (2000). VFPI: An isolation device for aseismic design. *Earthquake Engineering and Structural Dynamics, 29*(5), 603–627.

Robinson, W. H. (1982). Lead-rubber hysteretic bearings suitable for protecting structures during earthquakes. *Earthquake Engineering & Structural Dynamics, 10*(4), 593–604.

Saadatnia, M., Tajmir Riahi, H., & Izadinia, M. (2019). Hysteretic behavior of rubber bearing with yielding shear devices. *International Journal of Steel Structures, 19*(3), 747–759.

Sheikhi, J., Fathi, M., & Rahnavard, R. (2020). Natural rubber bearing incorporated with high toughness steel ring dampers. *Structures, 24*(C), 107–123.

Shenggang, F., Zhixia, D., Ganping, S., Chunfang, S., & Meijing, L. (2016). Experimental study on a new type of two-stage energy dissipation opening type low yield point steel energy dissipation device. *Journal of Southeast University (NATURAL SCIENCE EDITION), 46*(01), 110–117.

Steel Research; Study Results from Department of Architecture Update Understanding of Steel Research (Development and Cyclic Behavior of U-shaped Steel Dampers With Perforated and Nonparallel Arm Configurations). Journal of Technology, 2019.

Sun, J., Liu, K., Liu, G., Li, H. (2021). A developed transfer matrix method for analysis of elastic–plastic behavior of structures. *International Journal of Steel Structures*, *21*(5), 1620-1629. https://doi.org/10.1007/s13296-021-00524-8

Sun, J., Jiang, Y., Lv, G., Liu, K., Zhao, J. (2022a). Simulation analysis on seismic performance of assembled composite energy dissipation pipe joint. *International Journal of Steel Structures*, *22*(3), 880–893. https://doi.org/10.1007/s13296-022-00611-4

Sun, J., Qu, X., Gao, C. (2022b). Study on the design method of ring groove rivet joint in aluminum alloy structure. *International Journal of Steel Structures*, *22*(1), 294-307. https://doi.org/10.1007/s13296-021-00575-x

Sutcu F., Bal A., Fujishita K., Matsui R., Celik O.C., Takeuchi T. (2020). Comparing hysteretic behavior of RC frames retrofitted with low-yield-point (LYP) steel core BRB and perforated steel plate shear wall (PSPSW). In 14th World Conference on Earthquake Engineering.

Tian, J., Zhichao, Y., & Junlong, L. (2014). Study on seismic control of very low yield point steel in multi ribbed panel structures. *Vibration and Impact, 33*(05), 160–164.

Tianbo, P. E. N. G., Jianzhong, L. I., & Lichu, F. A. N. (2007). Development and application of double spherical aseismic bearing. *Journal of Tongji University (natural Science Edition), 35*(2), 176–180.

Tsai, C. S., Chiang, T. C., & Chen, B. J. (2003). Finite element formulations and theoretical study for variable curvature friction pendulum system. *Engineering Structures, 25*(14), 1719–1730.

Tsai, C. S., Chiang, T. C., & Chen, J. (2005). Experimental evaluation of piecewise exact solution for predicting seismic responses of spherical sliding type isolated structures. *Earthquake Engineering and Structural Dynamics, 34*(9), 1027–1046.

Tsai, H. G., & Hsueh, S. J. (2001). Mechanical properties of isolation bearings idented by a viscoelastic model. *International Journal of Solids and Structures, 38*(1), 53–74.

Tyler, R. G. (1977). Dynamic tests on PTFE sliding layers under earthquake conditions. *Bulletin of the New Zealand National Society for Earthquake Engineering, 10*(3), 129–138.

Wan-cheng, Y. U. A. N., Si-jie, W. A. N. G., Huai-feng, L. I., et al. (2021). Development of intelligence and resilience for bridge seismic design. *China Journal of Highway and Transport, 34*(2), 98–117.

Wan-cheng, Y. U. A. N., Xin-jian, C. A. O., & Zhao-jun, R. O. N. G. (2010). Development and experimental study on cable-sliding friction aseismic bearing. *Journal of Harbin Engineering University, 31*(12), 1593–1600.

Wang, R. Z., Chen, S. K., Liu, K. Y., et al. (2014). Analytical simulations of the steel-laminated elastomeric bridge bearing. *Journal of Mechanics, 30*(4), 373–382.

Weiqing, L., Zhuojun, M., Shuguang, W., & Dongsheng, D. (2016). Experimental study and numerical simulation of a new type of staged yielding mild steel damper. *Vibration and Shock, 35*(03), 87.

Xilin, L., Dayang, W., & Ying, Z. (2019). State-of-the-art of earthquake resilient structures. *Journal of Building Structures, 40*(2), 1–15.

Yan, S. H. I., Dong-sheng, W. A. N. G., Jan-ping, H. A. N., et al. (2017). Application status of seismic isolation for bridges and its development tendency. *Earthquake Engineering and Engineering Vibration, 37*(5), 118–128.

Yan, S. H. I., Hao-hao, W. A. N. G., Hong-guo, Q. I. N., et al. (2020). Deformation, heating and performance degradation of lead rubber bearings for highway bridges under near fault ground motions. *Journal of Vibration and Shock, 39*(23), 96–106.

Yan-lin, G. U. O., & Ming, Z. H. O. U. (2011). An overview of current state-of-the-art in behavior and design theory for unstiffened or buckling-restrained steel plate shear walls. *Journal of Building Structures, 32*(1), 1–16. in Chinese.

Zhang, L., Zhong-hua, L., & Xin-qiang, M. A. (2018). Study on parameter characteristics of rubber mooney-rivlin model. *Noise and Vibration Control, 38*, 427–430. in Chinese.

Zhouyi, C., Mai Chenglin, Xu., Zhixu, D. T., & Wei, H. (2019). Seismic behavior test of low yield point steel shear energy dissipation plate. *Journal of Xiamen University (NATURAL SCIENCE EDITION), 58*(06), 916–921.